TWO DIMENSIONAL HYDRODYNAMIC MODELLING OF A CIRCULATING FLUIDIZED BED RISER WITH SECONDARY AIR INJECTION-A TWO-FLUID APPROACH

Murat Koksal, Levent E. Ersoy, Feridun Hamdullahpur

Department of Mechanical Engineering, Dalhouise University
Halifax, Nova Scotia, B3J 2X4, Canada.

1. Introduction

Circulating fluidized bed (CFB) technology has been the subject of tremendous amount of research by many investigators for the last decade. Its superior characteristics over bubbling beds such as high slip velocities, improved radial mixing, reduced cross-sectional area for the same superficial gas velocity, less particle segregation and agglomeration have made this technology be utilized in a wide variety of industrial processes. Examples of such processes include combustion of coal, wood and shale, incineration of solid waste, gasification of coal, biomass, fluid catalytic cracking, desulfurization of flue gas (Grace et al., 1997). However, the understanding of the hydrodynamic behavior and heat transfer processes occurring in the CFBs is still incomplete due to complex flow phenomenon. Harris and Davidson (1994) classified the hydrodynamic modelling efforts in CFBs in three categories; models predicting only the axial solids suspension density (Type I), models predicting axial and radial solids hold-up and velocity profiles (Type II) and models using the fundamental equations of fluid mechanics (Type III). Type I and II models use the correlations based on the experimental data or combination of correlations and fundamental relationships. The type III models (also known as two-fluid models) are formulated in the framework of the Eulerian two-phase flow theory which is basically a generalization of Navier-Stokes equations used in single phase fluid mechanics. The main advantage of the two-fluid model is its applicability in problems involving complex flow phenomenon and geometry. The formulation of the two-fluid model begins with deriving the local instantaneous equations (mass, momentum and energy balances) and the interactions (also called jump conditions) between the phases for which several methods are available in the literature (Drew and Lahey, 1993; Ishii, 1975). These local instantaneous equations and the jump conditions are then averaged to get a solvable set of equations (Enwald et al., 1996) which must be closed by various closure laws. In this set of equations, each phase is characterized by its own mass, momentum and energy conservation equations hence the particle phase is modeled as a continuum.

In this context, the works of Gidaspow et al. (1989) and Tsuo and Gidaspow (1990) were the first to take the cluster formation into consideration and predict the core-annulus flow in a riser. Both of the studies used constant solid viscosity obtained from the experiments. In an other pioneering work, Ding and Gidaspow (1990) proposed a model that was capable of predicting the solids viscosity and the solids stress based on the kinetic theory of granular solids pioneered by Jenkins and Savage (1983), Lun et al. (1984), Johnson and Jackson (1987). Using this model, Gidaspow et al. (1992) simulated the entire CFB loop considering the return pipe and the solids inventory, which is basically an aerated bed. In a recent study, Samuelsberg and Hjertager (1996a) simulated a lab scale CFB with an ID of 0.032 m and compared the results with the data obtained from the laser Doppler anemometry. The velocity profiles from the simulations agreed well with the experimental data in the core region but the downflow near the walls were overpredicted. In another study, Samuelsberg and Hjertager (1996b) simulated the riser part of Illinois Institute of Technology CFB. The predicted solids velocity showed good agreement with the experimental data whereas the solid volume fraction showed some discrepancy near the inlet boundary. Recently, Niewland et al. (1996) extended the work of Ding and Gidaspow (1990) and simulated a lab scale riser with an ID of 0.0536 m.

The concept of secondary air arises from splitting the fluidization air into a primary air stream, which is injected axially from the bottom of the riser, and a secondary air stream injected laterally along the riser. The effects of staging the air in CFBs can vary from increased combustion efficiency, bed-to-wall heat transfer coefficients and reduced NO_x emissions to the alternation of the hydrodynamic regime in the riser (Basu 1991; Arena et al., 1993; Ersoy et al. 1997). A recent study by Ersoy et al. (1997) also shows considerable differences in particle axial velocity profiles for different modes of secondary air injection when compared to the cases without secondary air injection.

SA injection exhibits a complex flow structure which is influenced by a number of parameters such as SA/PA ratio, the injection port height and the injection mode. For this reason, modelling efforts are extremely

important to get a priori knowledge for design and operation purposes. The aim of this study is to present the preliminary results of the simulation of the radial secondary air injection on the riser hydrodynamics of a cold model lab scale CFB with ID of 0.23 m and a height of 7.6 m using a commercial software, Fluent V4.4. The computed axial particle velocity profiles and the suspension density in the riser are compared with the experimental measurements.

2. Governing Equations

The following equations in Cartesian tensor notation are obtained by ensemble averaging the local instantaneous equations and jump conditions and applying a phase-weighted averaging to the averaged equations (Enwald et al., 1997). With phase-weighted averaging, the cross correlation of the velocity fluctuations and the volume fraction fluctuations do not appear in the continuity equations unlike the case of non-weighted time averaging. Assuming no chemical reaction and isothermal condition, the following equations are written for the gas and the solid phase mass balances;

$$\frac{\partial(\varepsilon\rho)_g}{\partial t}+\frac{\partial(\varepsilon\rho U_i)_g}{\partial x_i}=0 \qquad [1]$$

$$\frac{\partial(\varepsilon\rho)_s}{\partial t}+\frac{\partial(\varepsilon\rho U_i)_s}{\partial x_i}=0 \qquad [2]$$

where subscripts s and g denote the solid and the gas phases, ε is volume fraction, ρ is the density, t is time and U is the mean velocity.

The gas phase momentum balance can be expressed as;

$$\frac{\partial(\varepsilon\rho U_j)_g}{\partial t}+\frac{\partial(\varepsilon\rho U_i U_j)_g}{\partial x_i}=-\varepsilon_g\frac{\partial P}{\partial x_j}+\frac{\partial(\varepsilon_g\tau_{ij,l})}{\partial x_i}+\frac{\partial(\varepsilon_g\tau_{ij,t})}{\partial x_i}+\varepsilon_g\rho_g g_j+K_{fs,j}(U_{j,s}-U_{j,g}) \qquad [3]$$

where P is the hydrostatic pressure, $\tau_{ij,l}$ is the laminar stress tensor, $\tau_{ij,t}$ is the turbulent stress tensor, g_j is the gravitational acceleration, and K_{fs} is the fluid-solid exchange (drag) coefficient. Equation 3 with $\varepsilon_g=1$ and $K_{fs}=0$ is the so-called Navier-Stokes equation.

The gas laminar stress tensor can be written as;

$$\tau_{ij,l}=\mu_l\left[\left(\frac{\partial U_j}{\partial x_i}+\frac{\partial U_i}{\partial x_j}\right)-\frac{2}{3}\delta_{ij}\frac{\partial U_k}{\partial x_k}\right] \qquad [4]$$

where μ_l is the shear viscosity and δ_{ij} is the Kroenecker delta.

The gas phase turbulent stress tensor following Boussinesq (1887) is;

$$\tau_{ij,t}=\mu_t\left[\left(\frac{\partial U_j}{\partial x_i}+\frac{\partial U_i}{\partial x_j}\right)-\frac{2}{3}\delta_{ij}\frac{\partial U_k}{\partial x_k}\right]-\rho\frac{2}{3}k\delta_{ij} \qquad [5]$$

where μ_t is turbulent eddy viscosity, k is the turbulent kinetic energy. In the present study, the value of the isotropic scalar turbulent eddy viscosity, μ_t, is computed from the standard single phase k-ε model in which no modifications are made in the transport equations for the turbulent kinetic energy, k, and dissipation, ε_d to model the effect of the dispersed phase. Near the wall, the turbulence is modeled by universal wall functions.

The solid phase momentum balance can be written as;

$$\frac{\partial(\varepsilon\rho U_j)_s}{\partial t}+\frac{\partial(\varepsilon\rho U_i U_j)_s}{\partial x_i}=-\varepsilon_s\frac{\partial P}{\partial x_j}+\frac{\partial(\varepsilon_s\tau_{ij,s})}{\partial x_i}++\varepsilon_s\rho_s g_j+K_{fs,j}(U_{j,g}-U_{j,})} \qquad [6]$$

where $\tau_{ij,s}$ is the solids stress tensor. In the above formulation, other forces such as added mass force, lift force and Basset force are neglected. The solid phase stress tensor is:

$$\tau_{ij,s}=\mu_s\left[\left(\frac{\partial U_j}{\partial x_i}+\frac{\partial U_i}{\partial x_j}-\frac{2}{3}\delta_{ij}\frac{\partial U_k}{\partial x_k}\right]-P_s\delta_{ij}+\xi_s\delta_{ij}\frac{\partial U_k}{\partial x_k}\right. \qquad [7]$$

where μ_s is the solid phase shear viscosity, ξ_s is the solid phase bulk viscosity, which describes the resistance of the solid phase to compression, and P_s is the solid phase pressure. The closures for these expressions are obtained from kinetic theory of granular solids.

Gas-Solid Drag:

The fluid-solid exchange coefficient, K_{fs}, has a form derived by Sylamlal and O'Brien (1993).

$$K_{fs} = \frac{3\varepsilon_s\varepsilon_g\rho_g}{4v_t^2 d_p} C_D\left(\frac{Re_p}{v_t}\right)\left|\vec{U}_s - \vec{U}_g\right| \qquad [8]$$

where Re_p is the particle Reynolds number, C_D is the drag coefficient, d_p is the particle diameter and v_t is the terminal velocity correlation as defined below.

$$Re_p = \frac{\rho_g d_p\left|\vec{U}_s - \vec{U}_g\right|}{\mu_g}, \qquad v_t = 0.5\left(A - 0.06\,Re_p + \sqrt{(0.06\,Re_p)^2 + 0.12\,Re_p(2B - A) + A^2}\right)$$

$A = \varepsilon_g^{4.14}$ and $B = 0.8\varepsilon_g^{1.28}$ for $\varepsilon_s \le 0.85$ and $B = \varepsilon_g^{2.65}$ for $\varepsilon_s > 0.85$ and $C_D = \left(0.63 + \frac{4.8}{\sqrt{Re_p/v_t}}\right)^2$

Solid Phase Pressure:

The solid phase pressure, P_s, represents the solid phase normal force due to particle interactions. It is considered as the sum of two effects, one corresponding to momentum transfer caused by particle velocity fluctuation correlations (kinetic term) and one caused by particle collisions. As suggested by Jenkins and Savage, (1983) Ding and Gidaspow, (1990), P_s is:

$$P_s = \varepsilon_s\rho_s\theta_s + 2\rho_s(1+e)\varepsilon_s^2 g_o\theta_s \qquad [9]$$

where e is the coefficient of restitution which describes the loss of kinetic energy after collision (e =1 is a perfectly elastic collision), g_o is the radial distribution function which can be interpreted as the probability of a single particle touching another particle of the solid phase (Boemer et al. 1997). θ_s is the so-called granular temperature, which describes the fluctuation kinetic energy of the particles. It is defined as;

$$\frac{3}{2}\theta_s = \frac{1}{2}\overline{C_s^2} \qquad [10]$$

where C_s is the fluctuating velocity of the solid phase.

The radial distribution function used in this study has the following form (Sylamlal et al., 1993).

$$g_o = \frac{1}{1-\varepsilon_s} + \frac{3\varepsilon_s}{2(1-\varepsilon_s)^2} \qquad [11]$$

Solid phase bulk viscosity (Ding and Gidaspow, 1990; Sylamlal et al., 1993; Balzer and Simonin, 1993):

$$\xi_s = \frac{4}{3}\varepsilon_s^2\rho_s d_p g_o(1+e)\sqrt{\frac{\theta_s}{\pi}} \qquad [12]$$

Solid phase shear viscosity:

The collisional part of the solid phase shear viscosity is due to the inter-particle forces. This part dominates in dense flows (Ding and Gidaspow, 1990; Sylamlal et al., 1993; Balzer and Simonin, 1993).

$$\mu_{s,coll} = \frac{4}{5}\varepsilon_s\rho_s d_p g_o(1+e)\sqrt{\frac{\theta_s}{\pi}} \qquad [13]$$

The kinetic contribution is modeled according to Sylamlal et al. (1993)

$$\mu_{s,kin} = \frac{\varepsilon_s d_p\rho_s\sqrt{\theta_s\pi}}{6(3-e)}\left[1 + \frac{2}{5}(1+e)(3e-1)\varepsilon_s g_o\right] \qquad [14]$$

Hence, the total solid phase shear viscosity is taken to be the sum of the collisional and kinetic parts.

Solids fluctuating (pseudo-thermal) energy balance (Ding and Gidaspow, 1990; Sylamlal et al., 1993; Balzer and Simonin, 1993):

$$\frac{3}{2}\left[\frac{\partial}{\partial t}(\varepsilon\rho\theta)_s + \frac{\partial(\varepsilon\rho U_i\theta)_s}{\partial x_i}\right] = \tau_{ij,s}\frac{\partial U_{j,s}}{\partial x_i} - \frac{\partial}{\partial x_i}\left[k_{\theta_s}\frac{\partial\theta_s}{\partial x_i}\right] - \gamma_{\theta_s} + \phi_{fs} \qquad [15]$$

where k_{θ_s} is the diffusion coefficient, γ_{θ_s}, is the dissipation of fluctuating energy due to particle collisions. The last term, ϕ_{fs}, represents the exchange of fluctuating energy between solid phase and the gas phase.

Following Lun et al. (1983);

$$\gamma_{\theta_s} = \frac{12(1-e^2)g_o}{d_p\sqrt{\pi}}\rho_s\varepsilon_s^2\theta_s^{3/2} \qquad [16]$$

and Sylamlal et al. (1993);

$$k_{\theta_s} = \frac{15 d_p \rho_s \varepsilon_s \sqrt{\theta\pi}}{4(41-33\eta)}\left[1+\frac{12}{5}\eta^2(4\eta-3)\varepsilon_s g_o + \frac{16}{15\pi}(41-33\eta)\eta\varepsilon_s g_o)\right] \quad \text{in which } \eta = 0.5(1+e)\,. \qquad [17]$$

and

$$\phi_{fs} = -3K_{fs}\theta_s \text{ (Gidaspow et al., 1992)} \qquad [18]$$

3. Experimental Study:

Figure 1 shows the schematics of the circulating fluidized bed assembly used in the experiments. Fluidization is maintained in the 0.23m ID, 7.6 m high Plexiglas column. A cyclone and a bag filter are used to collect the entrained solids. The details of the experimental set-up and the procedure can be found in Ersoy et al. (1997). For comparison with the simulation results, secondary air is injected at a height of 1.2 m from the distributor plate through two steel pipes of 0.0397 m ID. The injection planes are perpendicular to the riser axis. The SA/PA ratio was 0.5. The differential pressure measurement technique is used for voidage profile measurements in the riser. A data acquisition board, (National Instruments AT-MIO- 64E-3) is used to control the 32 pneumatic servo valves. Figure 1 shows the location of 8 pairs of static pressure taps placed along the riser. Data gathered from static pressure measurements are used to calculate the averaged solids holdup profile along the riser. When friction and acceleration effects are neglected the solids holdup, ε_s, in the riser can be approximated from ;

$$\Delta P = \rho_s g \Delta L \varepsilon_s \qquad [19]$$

An optical probe (Vector VSI- 2000) which is composed of two 1 mm diameter bundles of optical fiber spaced 4 mm apart was used for particle velocity measurements at three different locations; 0.93 m, 1.26 m and 1.83 m away from the distributor plate. The solid particles used in the experiments were FCC with mean particle diameter of 60 μm and a particle density of 1400 kg/m^3. External solids flow rate was measured by timing the amount of accumulated solids on a manually controlled flapper valve in the return leg.

4. Simulations:

The grid generation and the simulations were carried out by Fluent V4.4. The computational domain is illustrated in Figure 3. Due to excessive CPU time, only two simulations with SA/PA=0 and SA/PA=0.5 at a constant flux of 18 kg/m^{2}sec, were carried out. The superficial gas velocity was 3 m/s. The gas density and viscosity were 1.21 kg/m^3 and 1.79E-05 kg/m.s. The coefficient of restitution was 0.99. The total number of computational cells including the boundary cells were (37×56) 2072. The time step used in the simulations was 0.0005 s, which makes the average convective Courant number to be 0.007.

Boundary Conditions:

For the SA/PA=0 case, the fluidization air is fed from the bottom at a uniform velocity of 3 m/s. For SA/PA=0.5, the primary and the secondary air velocities are set to be 2 m/s and 2.875 m/s, respectively. This gives a SA/PA volumetric flowrate ratio of 0.5. Solids enter the riser from the side at a volume fraction of 5 %. The solid velocity is calculated as 0.257 m/s from the imposed solid flux. Initially, the domain is set to be devoid of particles. At the outlet of the riser, "outlet boundary" condition (all the fluxes vanish) is applied. The turbulent intensity of the gas is chosen to be 10 % at the primary and secondary air inlets. Fluent V4.4 uses zero flux for the granular temperature at the solid boundaries. "No slip" condition is used for the gas phase whereas the solid phase is allowed to slip on the walls.

Numerical Scheme:

A control volume based technique is employed to solve the conservation equations described for the model. In this technique, the domain is divided into discrete control volumes using a general curvilinear grid and the governing equations are integrated on the individual control volumes to construct the algebraic equations for discrete unknowns to be solved. The LGS (Line Gauss Seidel) method is used to solve the algebraic equations. For evaluation of the convective transport terms the power law scheme is used. The case with SA/PA = 0 was found to be more difficult to converge than the case with SA/PA=0.5 due to larger amounts of downflow near the walls which increased the transient behavior of the problem.

5. Results and Discussion:

All simulations were carried out for 30 s of real simulation time. The whole riser was filled up with the solids at the end of 9.5 s of real time simulation. The data in the last 5 s of the simulations were used for the time averaged particle axial velocity and solid suspension density profiles. Figure 4 shows the variation of the axial particle velocity during the last 2 s of the simulations for SA/PA=0 at different positions in the bed. As can be seen from the figure, although the solid flow at the upper part of the riser has reached a steady state, the axial velocity just near the solid inlet oscillates. This is an expected result because the bottom part of the riser is in the dense turbulent regime dominated by backflow of particles.

Figure 5 shows the comparison of the simulated suspension density and the one found from the pressure measurements along the riser height for SA/PA=0 and SA/PA=0.5. As observed in the experiments, secondary air injection divides the bed into a dense and a dilute region. The same trend is also captured in the simulations. This effect is more pronounced in the simulation results because the simulation is essentially 2-D but the actual secondary air injection is done in a 3-D geometry where the cut off effect is not as large as that of 2-D one. The suspension density comparisons show a large discrepancy at the bottom of the riser but the simulation results and the measurements get closer at the upper part of the riser. One of the reasons of this discrepancy may be the equation used to calculate the suspension density [19]. This equation is valid only at the fully developed region of the riser where the acceleration effects are not present. However, at the bottom of the riser, the pressure is balanced both by the weight and the acceleration of the particles. The second reason of the discrepancy between the experimental and simulated results may be the solid inlet conditions. As the exact experimental inlet conditions to the riser is unknown (solids are fed through a L-valve from the aerated bed), the simulated inlet conditions may differ from the experimental ones although the mass fluxes are the same.

Figures 6,7 and 8 show the variation of the experimental and the simulated particle axial velocity in the radial direction at heights of 0.93 m, 1.26 m and 1.82 m for SA/PA = 0 and SA/PA=0.5. Although, qualitatively, the trends are similar, the predicted values deviate from the experimental values. However, there are some interesting points that should be marked. Experiments show very small negative velocities near the wall (around - 0.5 m/sec) when compared to the simulated values (around -2 m/s) for SA/PA=0. One of the reasons of overpredicting the downflow near the wall may be the solid-wall boundary conditions. Solid-wall boundary conditions have always been problematic in two-fluid modelling. In this work, the solid phase is allowed to slip on the walls but the correct form would be to use a correlation which proposes a velocity between the two extremes; slip and no slip conditions like the one proposed by Sinclair and Jackson (1989). As the particle size increases, slip condition becomes more valid whereas for small particles no slip condition is favored. Unfortunately, Fluent V4.4 only allows slip and no slip conditions. Overpredicting the downflow near the wall was also noted by Samuelsberg and Hjertager (1996a). However, a core-annulus type of behavior is still observed at the bottom parts of the bed and the discrepancy between the experimental and simulated values decrease at the upper part of the riser (Figure 8). For SA/PA=0.5, a decrease in the value of the downflow velocity near the walls is noted. The secondary air injection at the height of 1.2 m, tends to cut off the backflow decreasing the amount of downflow. This effect can also be observed in Figure 2 which shows the instantaneous particle velocity vectors for SA/PA=0.5 and SA/PA=0 for the first 2.5 m of the riser height from the distributor plate. The effect of radial secondary air injection at the bottom of the riser can be clearly seen in this figure. In case of secondary air injection, the velocity profiles are flatter with more amount of downflow near the walls.

Secondary air injection affects the top parts of the riser as well (Figures 9 and 10) Unfortunately, there are no experimental velocity measurements for that region. Figures 9 and 10 show the variation of the time averaged solid volume fraction and axial velocity along the radial direction at 5.5 m away from the distributor plate for SA/PA=0 and SA/PA=0.5. A core-annulus type of behavior is satisfactorily predicted. The secondary air injection case has a slightly less solid volume fraction as seen in Figure 10. This is again due to cut off effect of the secondary air. The particle axial velocity in the core region for SA/PA=0 is higher than that of SA/PA=0.5 since more downflow is present in the former case.

More experimental validation at the top of the riser and work on the effect of mode of secondary air injection are underway.

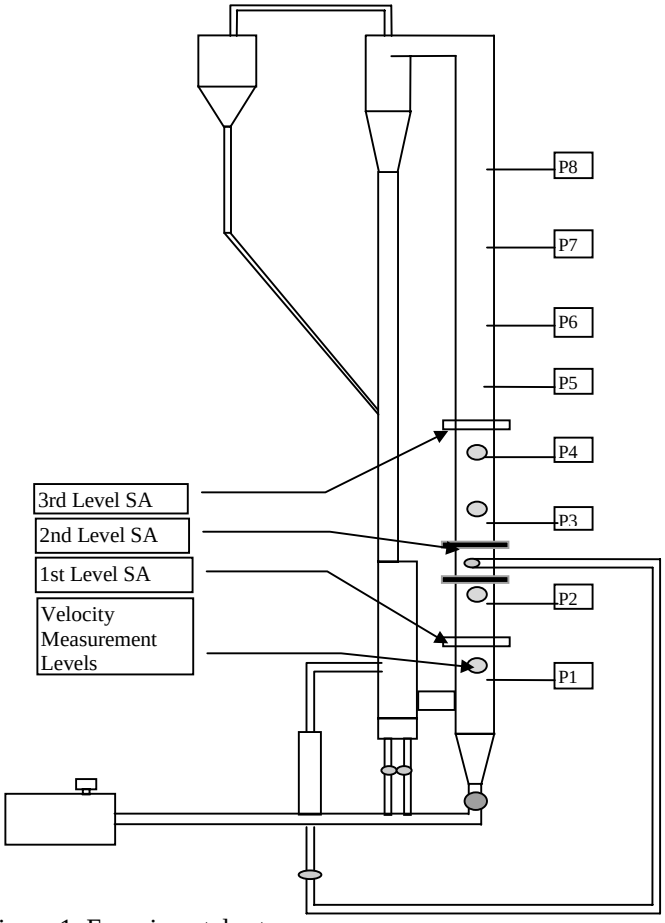

Figure 1. Experimental set-up.

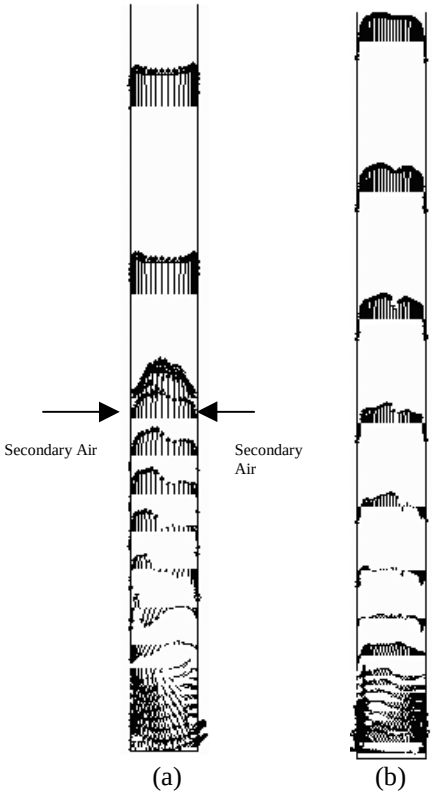

Figure 2. Instantaneous velocity vectors

a) SA/PA=0.5 b)SA/PA=0

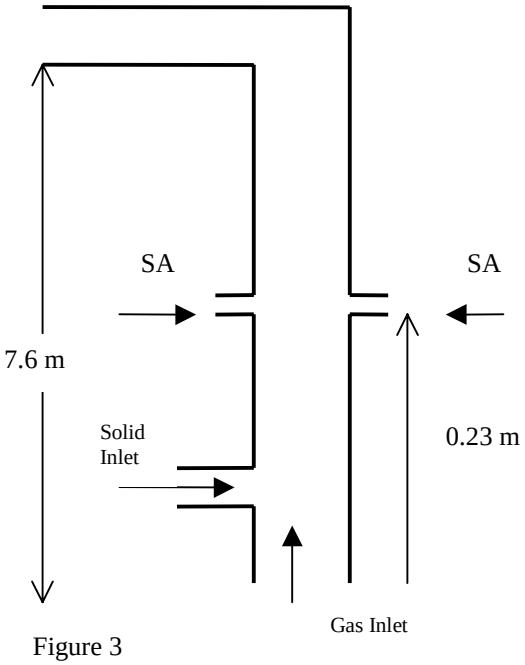

Figure 3

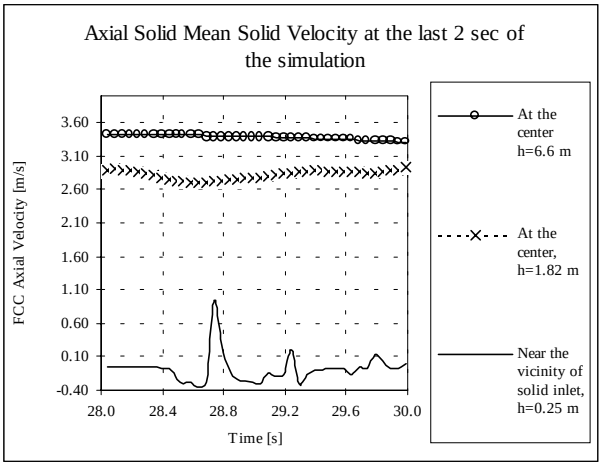

Figure 4. FCC Axial Velocity

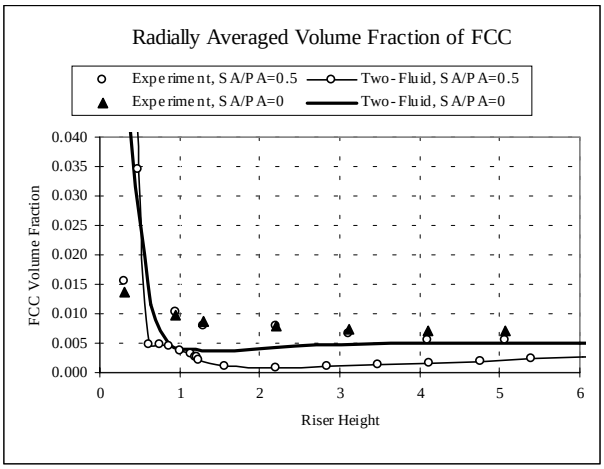

Figure 5. Radially Averaged FCC Suspension Density

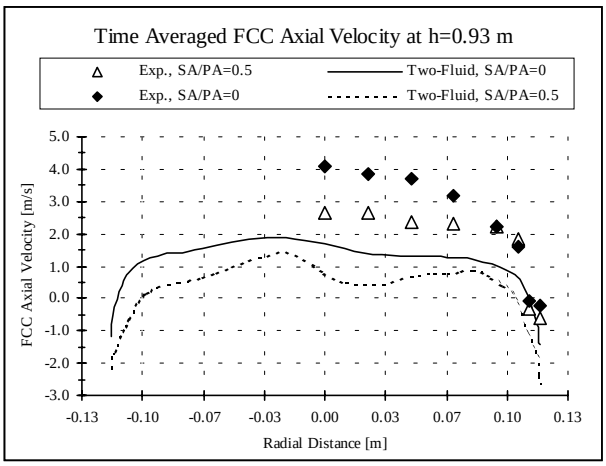

Figure 6. FCC Axial Velocity at h=0.93 m.

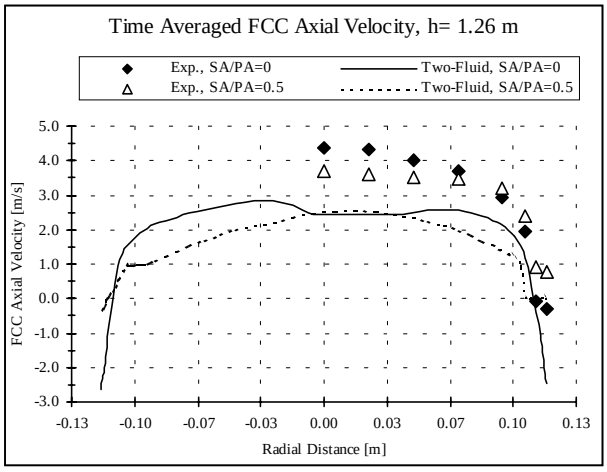

Figure 7. FCC Axial Velocity at h=1.26 m.

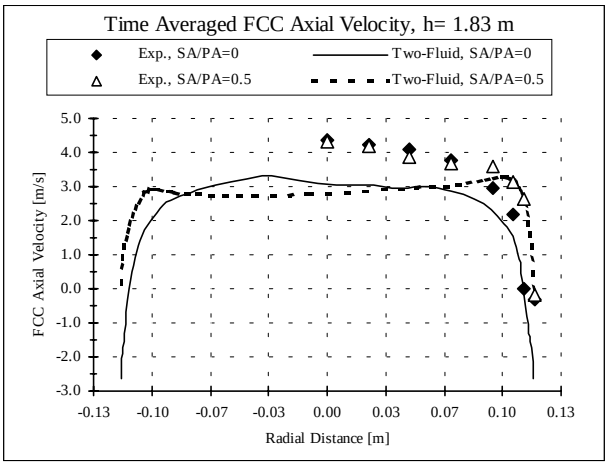

Figure 8. FCC Axial Velocity at h=1.83 m.

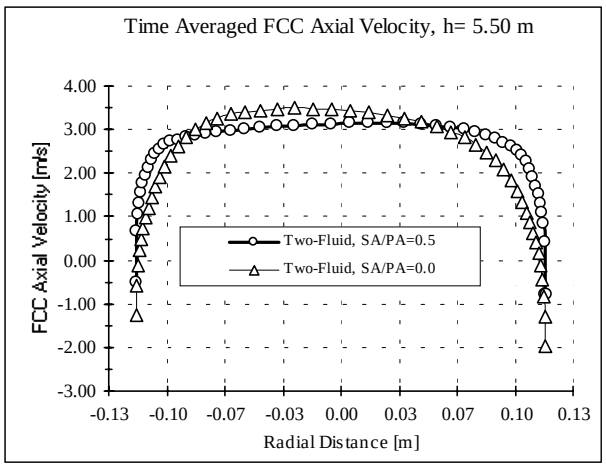

Figure 9. FCC Axial Velocity at h=5.5 m.

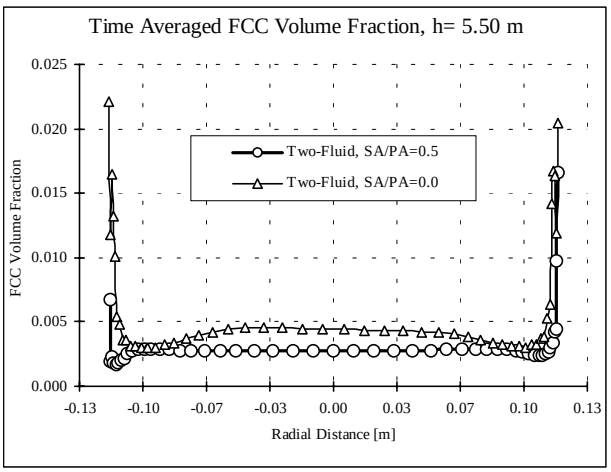

Figure 10. FCC Volume Fraction at h=5.5 m.

Acknowledgements- The simulations in this study were carried out by Fluent V4.4 which was provided by Fluent Inc. under educational license agreement.

6. References:

1) Arena, U., Camarota, A., Marzochella, A., Massimilla, L., *Fluidized Bed Combustion*, vol. 2., ASME, p.899-905, 1993.

2) Balzer, G., Simonin, O., "Extension of Eulerian Gas-Solid Flow Modelling to Dense Fluidized Bed", EDF, Report HE-44/93.13, 1993.

3) Basu, P., *Circulating Fluidized Bed Bolier, Design and Operation*, Butterworths-Heinemann-Reed Publishing Inc., Stoneham, MA., p. 182, 1991.

4) Boemer, A., Qi, H., Renz, U., "Eulerian Simulation of Bubble Formation at a Jet In a Two-Dimensional Fluidized Bed", Int. J. Multiphase Flow, vol. 23, no. 5, p. 927-944, 1997.

5) Ding, J., Gidaspow, D., "A Bubbling Fluidization Model Using Kinetic Theory of Granular Flow", AIChE J, vol. 36, no. 4, p. 523-538, 1990.

6) Drew, D.A., Lahey, R.T., *Particulate Two-Phase Flow*, Ch.16, p. 509-566, Butterworth-Heinemann, Boston, 1993.

7) Enwald, H., Peirano, E., Almstedt, A.E., "Eulerian Two-Phase Flow Theory Applied to Fluidization", Int. J. Multiphase Flow, vol. 22, Suppl., p. 21-66, 1996.

8) Ersoy, E.L., Militzer, J., Hamdullahpur, F., "Effect of Secondary Air Injection On the Hydrodynamics of Circulating Fluidized Beds", 14th FBC Conference, vol. 2, p. 1247, 1997.

9) Gidaspow, D., Bezbaruah, R., B., Ding, J., "Hydrodynamics of Circulating Fluidized Beds:Kinetic Theory Approach", eds., Potter, O.E., Nicklin, D.J., Fluidization VII, Engineering Foundation, p. 75-82, 1992.

10) Gidaspow, D., Tsuo, Y.P., Luo, K.M., "Computed and Experimental Cluster Formation and Velocity Profiles in Circulating Fluidized Beds", Fluidization IV, eds., Grace, J.R., Schemilt, L.W., Bergougnou, N.A., Engineering Foundation, p. 81-88, New York, 1989.

11) Grace, J.R., *Circulating Fluidized Beds*, eds., Grace, J.R., Avidan, A.A., Knowlton, T.M., Chapman & Hall, London, 1997.

12) Harris, B.J., Davidson, J.F., *Circulating Fluidized Bed Technology IV*, AIChE, New York, p. 32-39, 1994.

13) Ishii, M., *Thermo-fluid Dynamic Theory of Two-Phase Flow*, Eyrolles, Paris, 1975.

14) Jenkins, J.T., Savage, S.B., "A Theory for Rapid Flow of Identical, Smooth, Nearly Elastic Spherical Particles", J. Fluid Mechanics, vol. 130, p. 187, 1983.

15) Lun, C.K.K., Savage, S.B., Jeffrey, D.J., Chepurniy, N., "Kinetic Theories for Granular Flow:Inelastic Particles in Couette Flow and Slightly Inelastic Particles in a General Flow-Field", J. Fluid Mechanics, vol. 140, p. 223-256, 1984.

16) Nieuwland, J.J., Annaland, M.S., Kuipers, J.A.M., Swaaij, W.P.M., "Hydrodynamic Modelling of Gas/Particle Flows in Riser Reactors", AIChE J, vol. 42, no. 6, p. 1569-1582, 1996.

17) Samuelsberg, A., Hjertager, B.H., "An Experimental and Numerical Study of Flow Patterns in a Circulating Fluidized Bed Reactor", Int. J. Multiphase Flow, vol. 22, no. 3, p. 575-591, 1996a.

18) Samuelsberg, A., Hjertager, B.H., "Computational Modelling of Gas/Particle Flow in a Riser", AIChE J, vol. 42, no. 6, p. 1536-1546, 1996b.

19) Sinclair, J.L., Jackson, R., "Gas-Particle Flow in a Vertical Pipe with Particle-Particle Interactions", AIChE Journal, vol. 35, no. 9, p-1473-1486, 1989.

20) Syamlal, M., Rogers, W., O'Brian, T.J., "MFIX Documentation, Theory Guide", technical note DOE/METC-94/10004, 1993.

21) Tsuo, Y., Gidaspow, D., "Computation of Flow Patterns in Circulating Fluidized Beds", AIChE J, vol. 36, no. 6, p. 885-896, 1990.